

Mitigating Low-Frequency Bias: Feature Recalibration and Frequency Attention Regularization for Adversarial Robustness

Kejia Zhang^{1b}, Graduate Student Member, IEEE, Juanjuan Weng^{1b}, Yuanzheng Cai, Zhiming Luo^{1b}, Member, IEEE, Shaozi Li^{1b}, Senior Member, IEEE

Abstract—Ensuring the robustness of computer vision models against adversarial attacks is a significant and long-lasting objective. Motivated by adversarial attacks, researchers have devoted considerable efforts to enhancing model robustness by adversarial training (AT). However, we observe that while AT improves the models’ robustness against adversarial perturbations, it fails to improve their ability to effectively extract features across all frequency components. Each frequency component contains distinct types of crucial information: low-frequency features provide fundamental structural insights, while high-frequency features capture intricate details and textures. In particular, AT tends to neglect the reliance on susceptible high-frequency features. This low-frequency bias impedes the model’s ability to effectively leverage the potentially meaningful semantic information present in high-frequency features. This paper proposes a novel module called High-Frequency Feature Disentanglement and Recalibration (HFDR), which separates features into high-frequency and low-frequency components and recalibrates the high-frequency feature to capture latent useful semantics. Additionally, we introduce frequency attention regularization to magnify the model’s extraction of different frequency features and mitigate low-frequency bias during AT. Extensive experiments showcase the immense potential and superiority of our approach in resisting various white-box attacks, transfer attacks, and showcasing strong generalization capabilities.

Index Terms—Neural Network Robustness, Adversarial Training, Frequency.

I. INTRODUCTION

DNNs have achieved remarkable success in various applications across diverse domains. However, their susceptibility to inconspicuous adversarial perturbations [1]–[3] remains a substantial concern. These subtle perturbations, which are undetectable by the human eye, have the potential threat of resulting in erroneous predictions [4], [5]. As a consequence, the security and robustness of DNNs have become areas of widespread concern within both academic and industrial communities. Adversarial training (AT) [6]–[9] is widely acknowledged as one of the most effective techniques to enhance adversarial robustness of models. The AT accomplishes this

Kejia Zhang, Juanjuan Weng, Zhiming Luo, Shaozi Li are with the Department of Artificial Intelligence, Xiamen University, Xiamen 361005, China.

Yuanzheng Cai is with Fujian Provincial Key Laboratory of Information Processing and Intelligent Control, College of Computer and Control Engineering, Minjiang University, Fuzhou, 350108, China.

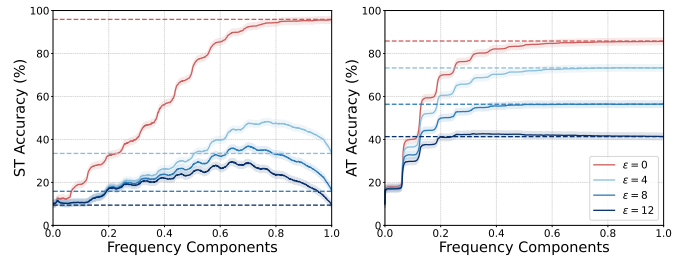


Fig. 1: Comparison analysis of simple training (ST, left) and adversarial training (AT, right) under various frequency ratios, considering inputs generated with different magnitudes of ϵ perturbations. “Frequency Components” refers to the proportion of frequency components retained during Fourier transformation.

by strategically integrating meticulously crafted adversarial examples (AEs) into the training process.

Despite the remarkable performance achieved by AT, relying solely on data augmentation using AEs appears insufficient to provide a comprehensive solution. Numerous studies have conducted an exploration of regularization [10], [11] or feature denoising [12], [13] approaches aimed at improving adversarial robustness. Recent advancements based on Fourier analysis [14]–[17] have underscored the potential of incorporating frequency analysis during AT to improve robustness. Motivated by these findings, Bu *et al.* [18] introduced an adaptive module to control frequency preferences, effectively adjusting the low-frequency and high-frequency components of feature representation. Yucel *et al.* [19] proposed a data augmentation method called HybridAugment that aims to mitigate the dependence of convolutional neural networks (CNNs) on high-frequency components. Furthermore, they propose HybridAugment++ as an attempt to consolidate various frequency-spectrum augmentations. However, it is important to recognize these approaches discard or suppress high-frequency components, which can lead to a significant loss of semantic information in the image [15].

In Figure 1, we illustrate the relationship between the proportion of feature frequency components and prediction accuracy during network inference. A Fourier transform is applied to the feature maps obtained after the initial convolutional layer to explore the impact of varying frequency components

on prediction accuracy. By preserving the minimum frequency components across different ratios and subsequently reconstructing the feature maps using the inverse Fourier transform, we can analyze the distinct contributions of various frequency components in feature derivation. We compare WRN32-10 trained with simple training (ST, Fig. 1 left) and adversarial training (AT, Fig. 1 right) on CIFAR-10 dataset. This figure provides empirical evidence that AT significantly improves the robustness of models. Based on the observations from the left in Fig. 1, we can find that adversarial perturbations on images lead to a decline in the model’s prediction accuracy when high-frequency features are present. This suggests that adversarial perturbations primarily affect the high-frequency domain of the features during the network’s inference process. Furthermore, we observe that the robustness achieved by AT does not imply an improved capacity to extract information from high-frequency components. Instead, it tends to bias the model towards relying more on low-frequency information while neglecting vulnerable high-frequency features.

Therefore, we propose a compelling perspective: the robustness of low-frequency and high-frequency features has distinct implications within the inference process of an AT-trained network. Specifically, the robustness of low-frequency features refers to the network’s capacity to effectively capture semantically valuable information for predictions, even when the low-frequency domain is compromised. On the other hand, the robustness of high-frequency features implies a reduced reliance of the network on high-frequency components, potentially resulting in sub-optimal performance in capturing subtle textures and intricate details [20].

Based on the above-discussed valuable insights, we raise a hypothesis: is it possible to improve the model’s robustness by utilizing high-frequency characteristics that undergo high-intensity perturbations? This entails capturing latent cues from high-frequency features and harmonizing the network’s feature extraction capabilities across various frequency domains. The objective of this approach is to recalibrate the high-frequency features and mitigate the low-frequency bias caused by AT.

To achieve this, we proposed a novel module “High-Frequency Disentanglement and Recalibration (HFDR)”. Firstly, HFDR employs high-pass filters to generate element-wise frequency attention maps, facilitating the disentanglement of features across different frequency domains. Then through the recalibration of vulnerable high-frequency features, the model effectively captures potential semantic cues within the high-frequency domain. The fusion of recalibrated high-frequency features with low-frequency features enhances the network’s ability to extract distinct frequency features. To further mitigate the low-frequency biases induced by AT, we introduce a frequency domain attention regularization. This regularization strategy aims to harmonize the network’s extraction capacity for different frequency domain information. Notably, our proposed model achieves comparable or superior robustness compared to state-of-the-art methods, while incurring minimal additional computational overhead.

In summary, this study makes the following three key contributions:

- Our research underscores a low-frequency bias in conven-

tional adversarial training methods during the network inference process. This robustness of these AT models is primarily established by disregarding vulnerable high-frequency features, which harbor valuable latent semantic information.

- We introduce an innovative module called High-Frequency Disentanglement and Recalibration (HFDR). This module enhances the model’s robustness by extracting latent valuable high-frequency cues and mitigates the low-frequency bias issue through incorporating frequency attention mechanisms.
- Our model achieves state-of-the-art performance in overall robustness with minimal additional cost and can be integrated with other adversarial training methods to enhance the model’s robustness.

II. RELATED WORK

A. Adversarial Attack

Deep neural networks (DNNs) demonstrate remarkable performance in various tasks by learning intricate relationships between inputs and outputs through complex, non-linear, and high-dimensional mappings. However, DNNs are susceptible to adversarial attacks, in which carefully crafted perturbation can deceive the model, leading to incorrect predictions. Several research studies have been dedicated to investigating the vulnerability of models and have proposed various advanced adversarial attack methods.

The Fast Gradient Sign Method (FGSM) [1] is a prominent attack technique that generates adversarial perturbations based on gradient signs. Madry *et al.* [21] developed the Projected Gradient Descent (PGD) attack method as a variant of FGSM, enabling a broader exploration of the adversarial sample space through iterative updating of FGSM. Carlini-Wagner *et al.* [22] introduced three novel attack methods employing L_0 , L_2 , and L_∞ distance metrics. Additionally, they proposed the use of high-confidence adversarial adversarial examples as a means to evaluate defense mechanisms. Croce *et al.* [23] introduced two extensions, namely APGD-CE and APGD-DLR, derived from PGD, to address challenges arising from sub-optimal step sizes and issues associated with the objective function. They further integrated these two attacks with two existing complementary attacks, FAB [24] and Square [25], and then introduced Auto-Attack (AA). AA has become a widely used approach for evaluating model robustness.

B. Adversarial Training Defense Methods

Adversarial training (AT) improves the robustness of models by incorporating adversarial examples into the training process, effectively defending against adversarial attacks. The conventional AT can be represented as a min-max optimization task, expressed mathematically as:

$$\min_{\theta} \mathbb{E}_{(x,y) \sim \mathcal{D}} \max_{\|\delta\|_p \leq \epsilon} \mathcal{L}(\theta; x + \delta, y), \quad (1)$$

where \mathcal{L} represents the loss function with respect to the model’s parameter θ , (x, y) is a clean image-label pair sampled

from the data distribution \mathcal{D} . Additionally, δ is a perturbation constrained by a maximum p -norm magnitude of ϵ .

The objective of the inner maximization is to generate adversarial examples, including attacks such as the PGD attack [21] and other attacks [26]–[30]. The outer minimization aims to develop effective training strategies for optimizing network parameters, thereby enhancing the model’s robustness against attacks. Rice *et al.* [31] conducted a study on the occurrence of overfitting in robust adversarial training and proposed employing a validation set protocol while performing model selection (PGD-AT):

$$\min_{\theta} \mathbb{E}_{(x,y) \sim \mathcal{D}} \max_{\|\delta\|_p \leq \epsilon} \mathcal{L}_{(CE)}(f_{\theta}(x + \delta), y), \quad (2)$$

Zhang *et al.* [32] categorized robust errors into “natural errors” and “boundary errors” to balance robustness and accuracy (TRADES):

$$\min_{\theta} \mathbb{E}_{(x,y) \sim \mathcal{D}} (\mathcal{L}_{(CE)}(f_{\theta}(x), y) + \beta \cdot \max_{\|\delta\|_p \leq \epsilon} \mathcal{L}_{(KL)}(f_{\theta}(x), f_{\theta}(x + \delta))), \quad (3)$$

Wang *et al.* [33] explicitly distinguished between misclassified and correctly classified examples during adversarial training (MART):

$$\min_{\theta} \mathbb{E}_{(x,y) \sim \mathcal{D}} (\mathcal{L}_{(BCE)}(f_{\theta}(x), y) + \beta \cdot \max_{\|\delta\|_p \leq \epsilon} \mathcal{L}_{(KL)}(f_{\theta}(x), f_{\theta}(x + \delta)) \cdot (1 - f_{\theta}(x))), \quad (4)$$

Wu *et al.* [34] introduced the Adversarial Weight Perturbation (AWP) to enhance the robustness of the model by considering the change in loss relative to the weight:

$$\min_{\theta} \mathbb{E}_{(x,y) \sim \mathcal{D}} \max_{\|\delta\|_p \leq \epsilon, \gamma \in \Gamma} (\mathcal{L}_{(CE)}(f_{\theta+\gamma}(x + \delta), y)), \quad (5)$$

Jia *et al.* [6] introduced a computationally intensive method, Learnable Attack Strategies Adversarial Training (LAS-AT), which involves automatically generating attack from strategy network g_{ω} and strategy set \mathcal{A} during the training process to enhance robustness:

$$\min_{\theta} \mathbb{E}_{(x,y) \sim \mathcal{D}} \max_{\omega} \mathbb{E}_{\mathcal{A} \sim p(\mathcal{A}|x;\omega)} \mathcal{L}_{(CE)}(f_{\theta}(x + g_{\omega}(x, \mathcal{A})), y), \quad (6)$$

These methods primarily rely on attack strategy redesign and optimization of the adversarial training process, often overlooking the analysis of feature properties during network inference.

C. Frequency Analysis for Robustness

Frequency analysis can be utilized to examine adversarial examples and their diverse frequency characteristics during the network inference process. Furthermore, frequency analysis aids in assessing the network’s robustness to various frequency features and their influence on the extraction of features. Yin *et al.* [14] demonstrated that data augmentation techniques enhance the robustness of the model against high-frequency distortions while reducing robustness against low-frequency distortions. Furthermore, they suggested that diverse data augmentation methods can alleviate this trade-off. Wang *et al.* [15]

emphasized that high-frequency components should not be considered mere noise; rather, CNNs can effectively leverage high-frequency information imperceptible to humans. Several studies have been influenced by frequency domain analysis and have introduced frequency-based approaches. Luo *et al.* [35] imposed low-frequency constraints to restrict adversarial perturbations in high-frequency components, thereby enhancing the stealthiness of attacks. Zhou *et al.* [36] introduced XNet, a semantic segmentation model for biomedical image analysis that incorporates both low-frequency and high-frequency information. Bu *et al.* [18] introduced a frequency preference control module that employs the Fourier transform to extract feature maps encompassing low-frequency signals, which facilitates the adjustment of the feature configuration. However, these methods have disregarded the existence of a low-frequency bias induced by adversarial training. Consequently, they do not effectively utilize and balance the extraction of high-frequency features. This imbalance ultimately results in the irreparable loss of valuable high-frequency information during network inference.

III. METHODOLOGY

Adversarial training can introduce an inherent low-frequency bias, which impedes the model’s capacity to effectively capture meaningful semantic information across diverse frequency domains. The root cause of this bias lies in the concentration of adversarial perturbations within the high-frequency domain. To tackle this concern, we present a novel “High-Frequency Disentanglement and Recalibration (HFDR)” Module as depicted in Figure 2. The HFDR module is formed of three key components: feature disentanglement, high-frequency feature recalibration, and frequency-based attention regularization.

Throughout the feature disentanglement phase (Section III-A), we generate feature attention maps to selectively focus on distinct frequency domains, facilitating the separation of features into their high-frequency and low-frequency components. The high-frequency feature recalibration stage (Section III-B) recalibrates the high-frequency information to effectively capture valuable semantic features. Additionally, we introduced an innovative regularization technique, termed “Frequency Attention Regularization”, to mitigate the low-frequency bias induced by Adversarial training (Section III-C).

A. Feature Disentanglement

Feature disentanglement refers to the process of separating and isolating different components or aspects within a given feature representation at a specific layer. In the context of network inference, let $\mathcal{X} \in \mathbb{R}^{(C \times H \times W)}$ represent the feature maps at a pre-defined layer, where C , H , and W are the channel, height, and width dimensions of \mathcal{X} , respectively. Drawing inspiration from the work of [37], we employ SRM filter [38] to extract high-frequency features. Subsequently, the channels are aligned through a 1×1 convolution, resulting in the formation of the high-frequency feature representation denoted as $\mathcal{X}_{HF} \in \mathbb{R}^{(C \times H \times W)}$. However, recent approaches commonly employ low-pass or high-pass filters for feature

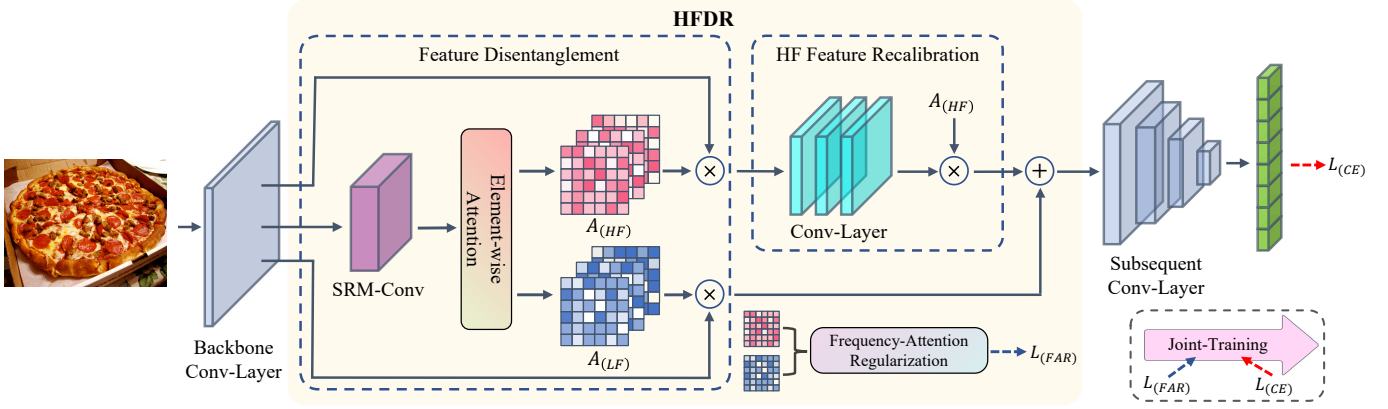


Fig. 2: During network inference, the input feature map undergoes the application of SRM filter and utilizes element-wise attention to generate the high-frequency attention map $A_{(HF)}$ and the low-frequency attention map $A_{(LF)}$. These maps are used to disentangle features into high and low-frequency components. After recalibrating the high-frequency features, they are combined with the low-frequency features before passing to subsequent network layers. To mitigate the low-frequency bias, a frequency-based attention regularization is further introduced.

disentanglement, resulting in the irreversible loss of information [39], [40].

In order to achieve feature disentanglement while minimizing information loss to the greatest extent possible, we propose employing filters to generate element-wise attention maps $A_i \in \mathbb{R}^{(C \times H \times W)}$, $i \in \{HF, LF\}$ for both high-frequency (HF) and low-frequency (LF) semantic sub-features. These attention maps are subsequently utilized to disentangle the features. To avoid the misconception about the enhanced model robustness is attributable to gradient masking, we integrate the Gumbel-Softmax method [41] for generating differentiable attention maps specifically for high-frequency components:

$$A_{(HF)} = \frac{\exp(g_{HF} + \log(\sigma(\mathcal{X}_{HF})/\tau))}{\sum_{j \in \{LF, HF\}} \exp(g_j + \log(\sigma(\mathcal{X}_j)/\tau))}, \quad (7)$$

where \mathcal{X}_j represents distinct semantic sub-features, and $\sigma(\cdot)$ denotes the sigmoid operation. The term g_j incorporates Gumbel noise, defined as $g_j = -\log(-\log(u_j))$ with $u_j \sim \mathcal{U}(0, 1)$. The term τ governs the impact of g_j . Additionally, the attention maps for low-frequency features can be computed as $A_{(LF)} = 1 - A_{(HF)}$.

In the context of attention maps $A_{(HF)}$ for high-frequency features, higher attention values indicate a prioritization of capturing semantic information linked to the high-frequency domain, while lower attention values suggest a diminished focus on high-frequency details within features. Leveraging frequency-based attention maps allows for the separation of weighted representations of the high-frequency feature $f_{(HF)} \in \mathbb{R}^{(C \times H \times W)}$ and the low-frequency feature $f_{(LF)} \in \mathbb{R}^{(C \times H \times W)}$, defined as:

$$\begin{cases} f_{(HF)} = \mathcal{X} \odot A_{(HF)}, \\ f_{(LF)} = \mathcal{X} \odot A_{(LF)}, \end{cases} \quad (8)$$

where \odot denotes the Hadamard product.

We acknowledge that adversarial perturbations primarily concentrate in the high-frequency domain. Neglecting these

critical inherent cues embedded in high-frequency information may result in missed opportunities for precise predictions. In the following sections, we will investigate the recalibration of high-frequency characteristics to capture valuable cues and semantic information.

B. High-Frequency Feature Recalibration

Previous studies [14], [42], [43] have demonstrated that adversarial perturbations mainly target the high-frequency features during network inference. To address this problem, several studies have employed low-pass filtering techniques to mitigate the impact of these high-frequency vulnerabilities and improve model robustness [40], [44]. Nonetheless, it is crucial to acknowledge that these high-frequency characteristics also encompass valuable latent cues for prediction tasks [42], [45].

Different from previous approaches, our objective is to empower robust models by enabling them to extract features from various frequency domains, rather than simply reducing reliance on vulnerable components. To accomplish this, after disentangling the features into low-frequency and high-frequency components, we suggest recalibrating the high-frequency features to effectively capture the latent semantic clues embedded within them, even in the presence of highly concentrated perturbations. As expressed by the equation below:

$$\tilde{f}_{(HF)} = \varphi(f_{(HF)}) \odot A_{(HF)}, \quad (9)$$

where φ represents the recalibration network, which is a three-layer convolutional network employed for feature extraction and transformation. The proposed method selectively modifies the activations of high-frequency features $f_{(HF)}$ to mitigate low-frequency biases during the recalibration process. $A_{(HF)}$ serves as a feature attention map to guide the network in the recalibration of high-frequency features, enhancing their discriminative representations. The recalibration network effectively learns and captures informative patterns from the input features through its convolutional layers. Following

the recalibration of the high-frequency features, we combine the recalibrated high-frequency features $\tilde{f}_{(HF)}$ with the low-frequency features $f_{(LF)}$ to generate the output feature maps $\tilde{f} = \tilde{f}_{(HF)} + f_{(LF)}$. This fusion process allows for the incorporation of both low and high-frequency information. By employing recalibration techniques, we are able to extract valuable predictive cues from high-frequency features that are vulnerable to attacks, while also mitigating potential low-frequency bias introduced by adversarial training.

C. Frequency Attention Regularization

Information within the feature map is represented at different frequencies: low-frequency conveys the global structure of image features, while high-frequency unveils the local details and structure. However, previous AT methods [18], [31], [33], [34], [46] often induced frequency biases during network inference. Without explicit guidance on network frequency preferences, the network may neglect the separated and refined high-frequency features $f_{(HF)}$.

Recall that we obtain the high-frequency attention map for each channel $\mathcal{H}\mathcal{F}_{(j)} = A_{HF}[j, :, :] \in \mathbb{R}^{(H \times W)}$, $j \in [1, C]$. We propose a straightforward method termed frequency attention regularization (FAR). The FAR aims to enhance the model’s ability to effectively extract both high-frequency and low-frequency features, while simultaneously mitigating inherent low-frequency bias during AT:

$$\mathcal{L}_{(FAR)} = \frac{1}{N \times C} \sum_{i,j} \left| \frac{\|\mathcal{H}\mathcal{F}_{(i,j)}\|}{\|1 - \mathcal{H}\mathcal{F}_{(i,j)}\|} - \beta \right|_p, \quad (10)$$

where $\mathcal{H}\mathcal{F}_{(i,j)}$ denotes the attention map for the j -th channel of the i -th image. N symbolizes the number of images, and C defines the number of channels in the feature maps processed by the HFDR module. Moreover, β serves as a balance factor that controls the ratio of information extraction between high-frequency and low-frequency components, while p indicates the norm exponent.

D. Model Training

Our proposed HFDR module can be easily integrated with existing AT methods, such as [31], [32], [34]. By combining the loss function $\mathcal{L}_{(FAR)}$ of the HFDR module with the conventional AT loss function, we derive our objective function as follows:

$$\mathcal{L} = \mathcal{L}_{(AT)} + \lambda \cdot \mathcal{L}_{(FAR)}, \quad (11)$$

where λ controls the influence of $\mathcal{L}_{(FAR)}$, and $\mathcal{L}_{(AT)}$ represents the loss function associated with various AT models. By integrating the HFDR module, we augment the capability of AT models to extract features across diverse frequency domains, thereby improving their adversarial robustness.

IV. EXPERIMENTS

A. Experimental Setup

Implementation Details: We evaluate the robustness of our approach by conducting experiments on the CIFAR-10 [47], CIFAR-100 [47], and Tiny Imagenet [48] datasets, utilizing

the WideResNet34-10 (WRN34-10) [49], AlexNet [17], and ResNet-18 (RN-18) [50] as the baseline models. For the implementation, we insert the HFDR module after the initial convolutional layer. To evaluate the impact of HFDR on improving the robustness of various AT techniques, our model was combined with three AT methods (PGD-AT [31], MART [33], AWP [34]), denoted as, HFDR-AT, HFDR-MART, and HFDR-AWP. We compared our approach with several baseline methods, including, PGD-AT [31], TRADES [32], AWP [34], MART [33], LBGAT [51], LAS-AT [6], FSR [52], FPCM [18], and CFA [53].

We trained WRN34-10 with identical hyperparameters and training details as specified in the original paper [31], [33], [34]. To ensure a fair comparison, we adopted the configuration of PGD-AT [31] as used in the experimental settings of FPCM [18], FSR [52] and CFA [53]. For ResNet18 and AlexNet, we initialized the learning rate to 0.1. The learning rate was subsequently reduced by a factor of 0.1 at the 90th and 95th epochs. The SGD optimizer with a momentum of 0.9 and a weight decay factor of $5e-4$ was employed for optimization. In the HFDR hyperparameter settings, we set $\lambda = 0.1$ and $\beta = 0.1$ for the loss term in Equation (10). The experiments were conducted on two NVIDIA RTX-A4000 GPUs.

Evaluation Settings: We evaluate the robustness of the model using various attack methods, including FGSM [1], PGD [31], CW [22], and AutoAttack [23]. Specifically, AutoAttack comprises APGD-DLR [23], APGD-CE [23], FAB [24], and Square [25]. These attacks are performed under the L_∞ norm with $\epsilon = 8$. Notice that, the ‘‘Clean’’ denotes the accuracy of clean test samples.

B. Comparison with Other Methods

In this part, we conducted a comparative analysis of the performance of our proposed module against other methods across diverse dataset conditions, encompassing varying resolutions and dataset sizes. Furthermore, we explored the efficacy of integrating our proposed module with different adversarial training techniques.

1) *Comparison on CIFAR-10 and CIFAR-100:* HFDR operates as a component that doesn’t necessitate intervention during adversarial training and can be integrated with other AT methods to improve robustness. Table I presents the efficacy of incorporating the HFDR module in elevating the model’s robustness. The key findings are as follows:

(1) HFDR improves the robustness of different adversarial training methods. After integrating our proposed HFDR module into the three baselines, the HFDR-AT, HFDR-MART, and HFDR-AWP can consistently outperform their corresponding baseline models across all attack scenarios, showcasing superior performance. For example, by incorporating HFDR into the PGD-AT method, we observe performance improvements of 2.60% in PGD-10, 1.22% in CW, and 2.07% in AA on CIFAR-10. Additionally, there is an increase in clean accuracy by 0.97% on CIFAR-100. Moreover, integrating the HFDR module into the MART and AWP methods also results in significant improvements in robust performance. The performance enhancement can be attributed to extracting valuable

TABLE I: Test robustness (%) using WRN34-10. The **number** in bold indicates the best accuracy.

Dataset	Method	Publish	Clean	PGD-10	PGD-20	PGD-50	C&W	AA
CIFAR-10	PGD-AT [31]	ICML-20	85.17	56.07	55.08	54.88	53.91	51.69
	TRADES [32]	ICML-19	85.72	56.75	56.10	55.90	53.87	53.40
	AWP [34]	NeurIPS-20	85.57	58.92	58.13	57.92	56.03	53.90
	MART [33]	ICLR-20	84.17	58.98	58.56	58.06	54.58	51.10
	LBGAT [51]	ICCV-21	88.22	56.25	54.66	54.30	54.29	52.23
	LAS-AT [6]	CVPR-22	86.23	57.64	56.49	56.12	55.73	53.58
	FSR [52]	CVPR-23	84.46	57.17	56.70	56.51	54.76	53.03
	FPCM [18]	ICCV-23	85.46	56.93	56.44	56.18	54.40	52.86
	CFA [53]	CVPR-23	84.90	57.78	57.35	56.81	54.56	52.63
	HFDR-AT		85.89	58.67	57.69	56.54	55.13	53.76
HFDR-MART	Ours	83.43	59.73	58.96	58.73	54.56	53.42	
HFDR-AWP		85.19	60.46	59.28	58.76	56.62	54.64	
CIFAR-100	PGD-AT [31]	ICML-20	60.89	32.19	31.69	31.45	30.10	27.86
	TRADES [32]	ICML-19	58.61	29.20	28.66	28.56	27.05	25.94
	AWP [34]	NeurIPS-20	60.38	34.13	33.86	33.65	31.12	28.86
	MART [33]	ICLR-20	59.23	33.10	32.77	32.56	30.32	28.57
	LBGAT [51]	ICCV-21	60.64	35.13	34.75	34.62	30.65	29.33
	LAS-AT [6]	CVPR-22	61.80	33.45	32.77	32.54	31.12	29.03
	FSR [52]	CVPR-23	59.41	33.76	33.33	32.94	30.40	28.56
	FPCM [18]	ICCV-23	60.97	32.57	32.18	32.90	30.27	28.15
	CFA [53]	CVPR-23	61.26	33.18	32.67	32.55	30.74	29.40
	HFDR-AT		61.86	35.23	34.61	34.29	31.13	30.27
HFDR-MART	Ours	60.16	35.94	35.60	35.41	32.07	30.98	
HFDR-AWP		59.17	36.90	36.42	36.13	32.59	31.74	

hidden semantics from high-frequency features that contain concentrated disturbances.

(2) Our model outperforms the baseline under attack. Our proposed model, HFDR-AWP, exhibits superior performance compared to all baseline methods, showcasing exceptional robustness. Specifically, HFDR-AWP outperforms the previous best baseline AWP by 1.77% of PGD-10, 1.51% of PGD-50, and 2.34% of AA on CIFAR-100. Besides, our method significantly outperforms the state-of-the-art frequency-based method, FPCM by a large margin. Unlike FPCM, which inserts multiple blocks into the network, we only inserted a single block, reducing the additional computation cost.

(3) HFDR impacts the generalization ability on clean samples. HFDR may introduce instability in the model’s generalization performance on clean samples. Specifically, we note that HFDR-AT improved clean accuracy on CIFAR-10 and CIFAR-100, with gains of 0.72% and 0.97%, respectively. Conversely, the HFDR-MART approach exhibits a decrease of 0.74% in clean sample accuracy on CIFAR-10, combined with a modest increase of 0.93% on CIFAR-100. One plausible explanation is that finer-grained and high-resolution data can help HFDR generate more distinctive attention maps, enabling effective recalibration. This ability allows the HFDR module to generate discriminative attention maps during network inference, enhancing the model’s capability to extract valuable cues from vulnerable high-frequency features.

TABLE II: Accuracy(%) on Tiny-Imagenet using ResNet18. The **number** in bold indicates the best accuracy.

Method	Clean	PGD-10	PGD-20	PGD-50	C&W	AA
PGD-AT [31]	44.15	21.45	21.08	20.91	18.74	16.13
MART [33]	45.13	23.41	22.37	22.17	18.91	16.32
AWP [34]	44.86	22.03	21.72	21.50	19.08	16.97
HFDR-AT	45.48	24.68	23.80	23.14	20.60	18.24
HFDR-MART	46.08	25.71	25.05	24.47	21.19	18.97
HFDR-AWP	45.67	26.69	25.28	24.61	22.55	19.27

2) *Comparison on Tiny ImageNet*: To evaluate the credibility and generalizability of the performance improvements, the corresponding performance results on the Tiny ImageNet [48] are presented in Table II. This dataset features higher resolution and a wider range of categories compared to CIFAR-10 and CIFAR-100. Specifically, the evaluation results on the Tiny ImageNet dataset reveal that HFDR-AT achieved performance enhancements of 1.86% and 2.11% against C&W and AA attacks, respectively, compared to PGD-AT. Furthermore, HFDR-AWP exhibited improvements of 3.47% and 2.30% when compared to AWP. These findings suggest that our approach seamlessly integrates with adversarial training frameworks, maintaining robust performance when confronted with complicate datasets.

TABLE III: Transfer attack accuracy (%) in the single-model transfer scenario. The **number** in bold indicates the best accuracy.

Attack ($\epsilon = 8$)	Performance w/o and w/ HFDR					
	Source: AlexNet			Source: WRN34-10		
	\Rightarrow ResNet50	\Rightarrow VGG16	\Rightarrow Inc-v3	\Rightarrow ResNet50	\Rightarrow VGG16	\Rightarrow Inc-v3
PGD-10	59.45/ 60.50	48.14/ 49.47	50.91/ 51.88	65.05/ 65.92	69.51/ 70.44	65.48/ 65.99
C&W	59.49/ 60.47	48.29/ 48.77	51.68/ 52.64	64.70/ 64.88	68.76/ 70.24	64.39/ 65.03
AA	60.82/ 62.34	53.45/ 54.01	56.31/ 57.01	70.47/ 71.53	66.97/ 68.85	67.16/ 69.34
SSA	35.30/ 36.76	32.88/ 33.62	37.57/ 38.61	44.63/ 45.91	48.91/ 50.35	43.84/ 44.58

C. Robustness to Transfer Attacks

In this part, we evaluated the performance of models equipped with the HFDR module against transfer attacks. When adversaries lack access to network parameters, they may employ alternative source models to craft adversarial examples for targeting the model under consideration. By scrutinizing the model’s robustness against transfer attacks, we aim to demonstrate that the enhancements in performance are not attributable to gradient masking. We conducted evaluations on the AlexNet and WRN34-10 models equipped with the HFDR module, utilizing techniques involving ResNet50, VGG16, Inception-v3 models, as well as PGD-10, C&W, AutoAttack (AA), and Spectrum Simulation Attack (SSA) to generate adversarial examples. The results of these assessments are presented in Table III, leading to the following conclusions:

(1) HFDR improve the robustness against various transfer attack. Models enhanced with the HFDR module have exhibited improved performance when encountering various transfer attacks generated by different source models. For instance, in scenarios involving source models ResNet50 and Inc-v3, the AlexNet equipped with HFDR showed a performance increase of 1.52% and 0.70% compared to the baseline model when exposed to AutoAttack (AA), while the WRN34-10 equipped with HFDR demonstrated performance gains of 1.06% and 2.18% when subjected to CW attacks. This observation further highlights that the performance enhancement achieved through our method is not attributed to gradient masking.

(2) HFDR improve the performance against the frequency-based attack. Furthermore, we evaluated the models’ robustness to frequency-domain attack SSA [43]. SSA employs discrete Fourier transform and inverse discrete Fourier transform to produce transferable attack instances. Specifically, when the AlexNet model, enhanced with the HFDR module, faced SSA attacks originating from ResNet50 and Inc-v3, the defense success rates improved by 1.46% and 1.04% respectively compared to the baseline approach.

D. Ablation Analysis

1) *Evaluation on HFDR module:* We evaluated the performance of using the disentanglement and recalibration process of high-frequency features (HFDR-Net) and adding the frequency attention regularization term (HFDR-FAR) in our proposed HFDR. From Table IV, we can find that:

(1) HFDR-Net capture latent high-frequency semantics. We observed that including the HFDR-Net network can lead

TABLE IV: Comparison of accuracy (%) with and without different HFDR components against various adversarial attacks. The **number** in bold indicates the best accuracy.

Method	Source: RN-18 Clean	Attack				
		FGSM	PGD-10	PGD-50	C&W	AA
Original	80.16	74.58	51.92	50.95	48.90	47.10
+HFDR-Net	80.58	75.73	53.74	52.95	50.99	47.83
+HFDR-FAR	81.27	76.64	54.69	53.58	51.86	48.33

TABLE V: Ablation analysis on the feature extract capability of various features obtained throughout HFDR-AT. “Method” represents the employed feature components for network inference during training. The **number** in bold indicates the best accuracy.

Method	Source: RN-18 Clean	Attack				
		FGSM	PGD-10	PGD-50	C&W	AA
f	80.16	74.58	51.92	50.95	48.90	47.10
$f_{(HF)}$	76.54	72.02	51.12	50.03	47.76	46.27
$f_{(LF)}$	78.54	73.14	51.41	51.67	47.86	46.13
$\tilde{f}_{(HF)}$	79.67	74.43	52.21	51.40	48.14	46.82
$\tilde{f}_{(ours)}$	81.27	76.64	54.69	53.58	51.86	48.33

to significant improvements in the standard accuracy and robustness of our model. This discovery not only confirms the potential of capturing predictive semantic information from high-frequency features but also indirectly validates the limitations of traditional adversarial training methods in extracting high-frequency features.

(2) HFDR-Regularization mitigate low-frequency bias. Incorporating frequency domain attention-based regularization has led to enhancements across various metrics. For instance, compared to the scenario without this loss term, the performance of PGD-10 attack and AA attack has shown respective increases of 0.95% and 0.60%. This highlights the efficacy of frequency domain attention regularization in mitigating low-frequency biases during adversarial training.

2) *Effectiveness of different frequency components:* We analyzed the role played by the different frequency components of HFDR in the disentanglement and recalibrating process during network inference. From Table V, we can find that:

(1) Leveraging only high-frequency features can yield high accuracy. The experimental results demonstrate that a classification accuracy of 76.56% can be achieved, even when utilizing solely uncalibrated high-frequency features $h_{(HF)}$.

TABLE VI: The effect of HFDR with DFT high-pass filter. The **number** in bold indicates the best accuracy.

Method	Clean	Attack				
		FGSM	PGD-10	PGD-50	C&W	AA
N/A	80.16	74.58	51.92	50.95	48.90	47.10
DFT(B=8)	81.11	75.99	55.25	52.16	50.45	47.81
DFT(B=16)	81.12	76.07	54.02	51.21	49.97	47.60
SRM(Ours)	81.27	76.64	54.69	53.38	51.86	48.33

TABLE VII: The effect of HFDR at different layers. The **number** in bold indicates the best accuracy.

Method	Clean	Attack				
		FGSM	PGD-10	PGD-50	C&W	AA
Conv.1 (Ours)	85.89	78.35	58.67	56.54	55.13	53.76
Conv.2	85.52	77.96	57.86	55.70	54.32	52.79
Conv.3	84.73	77.54	56.92	55.56	54.30	52.40
Conv.4	84.59	77.43	57.13	55.60	54.14	52.21

These features also exhibited robustness against PGD-10 (51.12%) and AA (46.27%). The findings of this study provide additional confirmation of the viability of our work, demonstrating that the network possesses the ability to accurately capture semantically significant information for prediction from high-frequency features, even when subjected to highly concentrated perturbations.

(2) Recalibration effectively captures valuable high-frequency features. Compared to $f_{(HF)}$, training with the recalibrated high-frequency features $\tilde{f}_{(HF)}$ yielded improvements of 2.41% and 1.09% under the FGSM and PGD-10 attacks, respectively. This demonstrates that our recalibration stage effectively captures valuable semantics that enhance the predictive capabilities of the model.

(3) HFDR harmonizes the extraction of high-frequency and low-frequency features. By employing HFDR module to obtain $\tilde{f} = \tilde{f}_{(HF)} + f_{(LF)}$, we observed significant improvements in multiple performance aspects compared to the initial features $f = f_{(HF)} + f_{(LF)}$. For example, \tilde{f} exhibits enhancements of 2.77% and 1.23% under PGD-10 and AA attacks, respectively.

3) *Effectiveness of different frequency filtering*: The effectiveness of feature disentanglement using various frequency domain filtering methods is examined in Table VI. Specifically, the DFT-based approach involves processing data transformed by the Discrete Fourier Transform, where the spectral central width is denoted as B. In this procedure, frequency components located outside of a spectral central square are zeroed out, followed by the utilization of the inverse Discrete Fourier Transform for filtering. The findings suggest that high-pass filters with a smaller central width B exhibit a more improved performance. This can be attributed to its enhanced capability to separate high-frequency features from image features. By focusing on the high-frequency components that capture intricate and distinctive details, the filter DFT(B=8) augment the model’s ability to extract subtle patterns and variations in the data during feature disentanglement, leading to an improved performance in feature recalibration. Nevertheless, these results do not surpass the performance of the SRM filter.

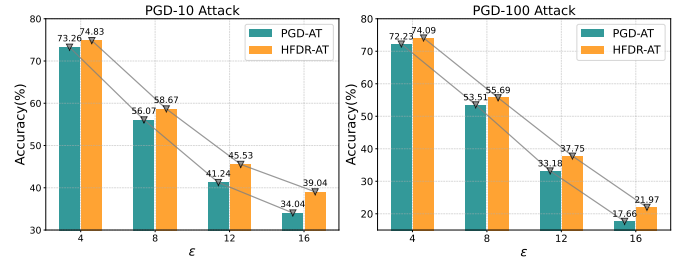


Fig. 3: Comparisons with varying ϵ values using WRN34-10 on the CIFAR-10. The x -axis represents the ϵ value, while y -axis represents the robust accuracy (%).

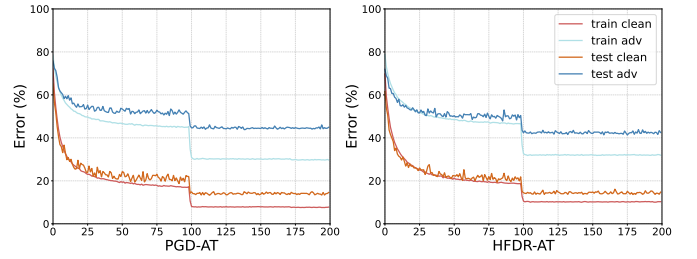


Fig. 4: The learning curves for clean and robust accuracy on the training and test sets of CIFAR-10 using WRN34-10.

4) *Robustness at Different HFDR Positions*: The robustness of WRN34-10 with diverse HFDR module placements is presented in Table VII. The outcomes reveal that integrating the HFDR module after Conv.1 leads to exceptional robust and clean performance. This effect is attributed to the relationship between the network’s depth and the level of abstraction in the extracted features. Features with shallower depths and lower levels of abstraction are better suited for discerning different frequency characteristics during feature decoupling, allowing the HFDR module to perform more effective high-frequency feature calibration.

E. Robust Generalization Analysis

1) *Robustness under Various ϵ Attacks*: We investigated the robustness of our proposed HFDR module under different levels of attack intensity. From the results in Fig. 3, we can have the following observations:

(1) HFDR enhances robustness against adversarial attacks. Our proposed method demonstrates improved performance against FGSM and PGD-10 attacks across different values of ϵ . For example, under the PGD-10 attack, HFDR-AT shows respective increases of 1.57%, 2.60%, 4.29%, and 5.00% compared to PGD-AT at ϵ values of 4, 8, 12, and 16.

(2) HFDR enhances the generalization against attacks. As the value of ϵ increases, our method demonstrates improved generalization capabilities by exhibiting a smaller decrease in accuracy compared to the baseline approach. For instance, when ϵ increases from 8 to 16, PGD-AT experiences a 22.03% decrease in accuracy, whereas HFDR-AT only observes a 19.63% decline under the PGD-10 attack.

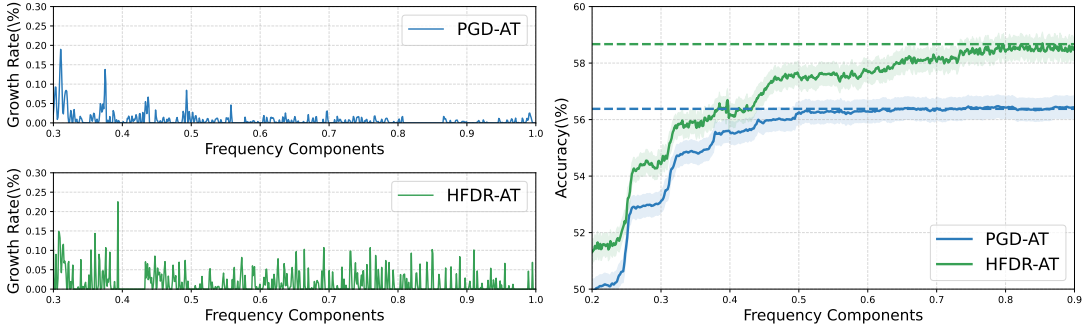


Fig. 5: Comparison of growth rate (%) and robust accuracy (%) under PGD-10 attack ($\epsilon = 8$) between HFDR-AT and PGD-AT methods across increasing frequency components.

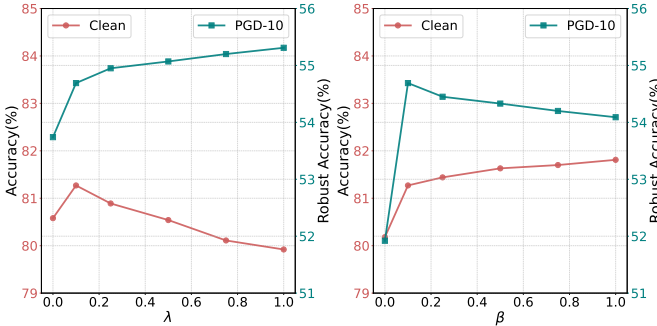


Fig. 6: Analysis of hyper-parameters λ and β using ResNet-18 on CIFAR-10. The x -axis represents the parameter value, while y -axis represents the accuracy(%).

2) *Robust Generalization Gap*: Our investigation delved into the influence of HFDR on the deviation in robust generalization during the training process. We extended the training epochs to 200 to enhance the visualization effect, as illustrated in Fig. 4. It is evident that HFDR-AT significantly alleviates overfitting in the model during training in comparison to PGD-AT. Furthermore, it diminishes both the discrepancy in robust generalization gap and standard generalization gap, thereby enhancing the model’s generalization capability.

F. Parameter Sensitive Analysis

In this part, we performed an analysis of the HFDR module hyper-parameters. In Figure 6, a visualization of parameter sensitivity for hyperparameters λ and β in the HFDR method is demonstrated. Notably, assigning a value of zero to β results in the absence of the frequency attention regularization term (refer Equation (10)). Evidence suggests that these two hyper-parameters influence the trade-off between model clean and robust accuracy performance. The following offers a detailed analysis:

(1) The parameter λ determines the magnitude of the frequency attention regularization term. As the parameter λ increases, there is a corresponding rise in robust accuracy, contrasted by a decline in clean accuracy. When the value of β is maintained constant, an increase in λ causes the the adversarial training focus on high-frequency separation,

TABLE VIII: Comparison of computational costs (# Params and Times) between the original model and our approach on CIFAR-10.

Method	<i>WRN34-10</i>		<i>ResNet-18</i>	
	# Params (M)	Times (s)	# Params (M)	Times (s)
Original	46.16	1050	11.17	247
+HFDR	46.21	1068	11.29	260

, which can slightly compromising the model’s capability to extract features from clean examples. However, a larger λ value facilitates the disentanglement of high-frequency components during network inference, thereby enhancing the model’s capability to recalibrate perturbed high-frequency features. To strike an optimal balance between model robustness and clean accuracy, it is recommended to set $\lambda = 0.1$.

(2) The parameter β influences the extraction of high-frequency features. Increasing β typically reduces robust accuracy while enhancing clean accuracy. Notably, the model performs better when the frequency attention regularization term is activate (*i.e.* $\beta \neq 0$). As β increases, $f_{(HF)}$ retains more high-frequency feature information, improving the model’s ability to recalibrate these informative features in clean images. Conversely, adversarial attacks introduce perturbations that disrupt high-frequency features, complicating their recalibration. Therefore, a balanced setting, such as $\beta = 0.1$, is recommended.

G. Analysis of Mitigation of Low-Frequency Bias

In this part, we delve into exploring the mitigating effects of our proposed module HFDR on low-frequency biases during adversarial training. In Figure 5, we showcased the efficacy of our HFDR-AT method in extracting diverse frequency domain features compared to PGD-AT. The left figure illustrates that the growth trend in model performance with the incorporation of low to high-frequency features, whereas the right figure depicts variations in model performance with the incorporation of low to high-frequency components. These findings suggest that our model exhibits an enhanced proficiency in extracting high-frequency features. Specifically, our model can recalibrate the perturbed high-frequency features to alleviate the low-frequency bias caused by traditional adversarial training.

H. Computational Efficiency

Table VIII depicts the comparison of our approach and the original model in terms of training efficiency. This comparison includes the analysis of the model parameters and the average time required for one training cycle. The results highlight that our model enhances the robustness of the model without a significant increase in model parameters or the cost of AT. For instance, on the CIFAR-10, the regular WRN34-10 takes 1,050 seconds for one training cycle, whereas the model with HFDR only takes 1,068 seconds. This demonstrates the clear advantages of our model compared to other methods with complex network architectures.

V. CONCLUSION

In this paper, we propose a module called High-Frequency Disentanglement and Recalibration (HFDR) to tackle the issue of low-frequency bias arising from adversarial training, which comprises three key components: feature disentanglement and recalibration with frequency domain attention regularization. We achieve this by leveraging frequency domain attention maps to separate feature maps into low-frequency and high-frequency components and then recalibrating the high-frequency features. This recalibration enhances the model's robustness by incorporating valuable semantic clues for accurate prediction. Additionally, we utilize frequency domain attention regularization to ensure a balanced extraction of features with different frequencies during the derivation process, thereby mitigating the low-frequency bias associated with traditional adversarial training. Extensive experiments verified the effectiveness of our method.

On the other aspect, this paper could provide a notable guiding direction for future research on model robustness. We introduce a novel perspective that emphasizes the importance of the robustness of feature extraction capability in achieving outstanding model robustness. In other words, when confronted with perturbations across various frequency domain features, a robust model should consistently extract valuable semantic information from these features rather than neglecting the robustness provided by features with high-density perturbation frequencies.

REFERENCES

- [1] I. J. Goodfellow, J. Shlens, and C. Szegedy, "Explaining and harnessing adversarial examples," *arXiv preprint arXiv:1412.6572*, 2014.
- [2] Y. Zhu, Y. Chen, X. Li, R. Zhang, X. Tian, B. Zheng, and Y. Chen, "Information-containing adversarial perturbation for combating facial manipulation systems," *IEEE Trans. Inf. Forensics Security*, vol. 18, pp. 2046–2059, 2023.
- [3] S. Jia, B. Yin, T. Yao, S. Ding, C. Shen, X. Yang, and C. Ma, "Adv-attribute: Inconspicuous and transferable adversarial attack on face recognition," in *Proc. Adv. Neural Inform. Process. Syst. (NeurIPS)*, vol. 35, 2022, pp. 34 136–34 147.
- [4] T. Fel, M. Ducoffe, D. Vigouroux, R. Cadène, M. Capelle, C. Nicodème, and T. Serre, "Don't lie to me! robust and efficient explainability with verified perturbation analysis," in *Proc. IEEE/CVF Conf. Comput. Vis. Pattern Recog. (CVPR)*, 2023, pp. 16 153–16 163.
- [5] S. J. Oh, M. Fritz, and B. Schiele, "Adversarial image perturbation for privacy protection a game theory perspective," in *Proc. IEEE/CVF Int. Conf. Comput. Vis. (ICCV)*, 2017, pp. 1491–1500.
- [6] X. Jia, Y. Zhang, B. Wu, K. Ma, J. Wang, and X. Cao, "Las-at: adversarial training with learnable attack strategy," in *Proc. IEEE/CVF Conf. Comput. Vis. Pattern Recog. (CVPR)*, 2022, pp. 13 398–13 408.
- [7] M. Andriushchenko and N. Flammarion, "Understanding and improving fast adversarial training," in *Proc. Adv. Neural Inform. Process. Syst. (NeurIPS)*, vol. 33, 2020, pp. 16 048–16 059.
- [8] H. Kuang, H. Liu, X. Lin, and R. Ji, "Defense against adversarial attacks using topology aligning adversarial training," *IEEE Trans. Inf. Forensics Security*, 2024.
- [9] G. Jin, X. Yi, D. Wu, R. Mu, and X. Huang, "Randomized adversarial training via taylor expansion," in *Proc. IEEE/CVF Conf. Comput. Vis. Pattern Recog. (CVPR)*, 2023, pp. 16 447–16 457.
- [10] J. Tack, S. Yu, J. Jeong, M. Kim, S. J. Hwang, and J. Shin, "Consistency regularization for adversarial robustness," in *Proc. AAAI Conf. Artif. Intell.*, vol. 36, no. 8, 2022, pp. 8414–8422.
- [11] D. Yang, I. Kong, and Y. Kim, "Enhancing adversarial robustness in low-label regime via adaptively weighted regularization and knowledge distillation," in *Proc. IEEE/CVF Int. Conf. Comput. Vis. (ICCV)*, 2023, pp. 4552–4561.
- [12] G. Li, S. Ding, J. Luo, and C. Liu, "Enhancing intrinsic adversarial robustness via feature pyramid decoder," in *Proc. IEEE/CVF Conf. Comput. Vis. Pattern Recog. (CVPR)*, 2020, pp. 800–808.
- [13] M. Guo, Y. Yang, R. Xu, Z. Liu, and D. Lin, "When nas meets robustness: In search of robust architectures against adversarial attacks," in *Proc. IEEE/CVF Conf. Comput. Vis. Pattern Recog. (CVPR)*, 2020, pp. 631–640.
- [14] D. Yin, R. Gontijo Lopes, J. Shlens, E. D. Cubuk, and J. Gilmer, "A fourier perspective on model robustness in computer vision," in *Proc. Adv. Neural Inform. Process. Syst. (NeurIPS)*, H. Wallach, H. Larochelle, A. Beygelzimer, F. d'Alché-Buc, E. Fox, and R. Garnett, Eds., vol. 32, 2019.
- [15] H. Wang, X. Wu, Z. Huang, and E. P. Xing, "High-frequency component helps explain the generalization of convolutional neural networks," in *Proc. IEEE/CVF Conf. Comput. Vis. Pattern Recog. (CVPR)*, 2020, pp. 8684–8694.
- [16] C. Xue, Z. Tian, F. Zhan, S. Lu, and S. Bai, "Fourier document restoration for robust document dewarping and recognition," in *Proc. IEEE/CVF Conf. Comput. Vis. Pattern Recog. (CVPR)*, 2022, pp. 4573–4582.
- [17] Y. Wang, Y. Wu, S. Wu, X. Liu, W. Zhou, L. Zhu, and C. Zhang, "Boosting the transferability of adversarial attacks with frequency-aware perturbation," *IEEE Trans. Inf. Forensics Security*, pp. 1–9, 2024.
- [18] Q. Bu, D. Huang, and H. Cui, "Towards building more robust models with frequency bias," in *Proc. IEEE/CVF Int. Conf. Comput. Vis. (ICCV)*, 2023, pp. 4402–4411.
- [19] M. K. Yucel, R. G. Cinbis, and P. Duygulu, "Hybridaugment++: Unified frequency spectra perturbations for model robustness," in *Proc. IEEE/CVF Int. Conf. Comput. Vis. (ICCV)*, 2023, pp. 5718–5728.
- [20] M. Oechsle, L. Mescheder, M. Niemeyer, T. Strauss, and A. Geiger, "Texture fields: Learning texture representations in function space," in *Proc. IEEE/CVF Int. Conf. Comput. Vis. (ICCV)*, 2019, pp. 4531–4540.
- [21] A. Madry, A. Makelov, L. Schmidt, D. Tsipras, and A. Vladu, "Towards deep learning models resistant to adversarial attacks," in *Proc. Int. Conf. Learn. Represent. (ICLR)*, 2018.
- [22] N. Carlini and D. Wagner, "Towards evaluating the robustness of neural networks," *IEEE Symp. Security Privacy*, pp. 39–57, 2017.
- [23] F. Croce and M. Hein, "Reliable evaluation of adversarial robustness with an ensemble of diverse parameter-free attacks," in *Proc. Int. Conf. Mach. Learn. (ICML)*, vol. 119, 2020, pp. 2206–2216.
- [24] —, "Minimally distorted adversarial examples with a fast adaptive boundary attack," in *Proc. Int. Conf. Mach. Learn. (ICML)*, 2020, pp. 2196–2205.
- [25] M. Andriushchenko, F. Croce, N. Flammarion, and M. Hein, "Square attack: a query-efficient black-box adversarial attack via random search," in *Proc. Eur. Conf. Comput. Vis. (ECCV)*, 2020, pp. 484–501.
- [26] L. Chen, Y. Zhang, Y. Song, L. Liu, and J. Wang, "Self-supervised learning of adversarial example: Towards good generalizations for deepfake detection," in *Proc. IEEE/CVF Conf. Comput. Vis. Pattern Recog. (CVPR)*, 2022, pp. 18 710–18 719.
- [27] X. Wei, Y. Guo, and J. Yu, "Adversarial sticker: A stealthy attack method in the physical world," *IEEE Trans. Pattern Anal. Mach. Intell.*, vol. 45, no. 3, pp. 2711–2725, 2022.
- [28] J. Byun, S. Cho, M.-J. Kwon, H.-S. Kim, and C. Kim, "Improving the transferability of targeted adversarial examples through object-based diverse input," in *Proc. IEEE/CVF Conf. Comput. Vis. Pattern Recog. (CVPR)*, 2022, pp. 15 244–15 253.
- [29] J. Zou, Y. Duan, B. Li, W. Zhang, Y. Pan, and Z. Pan, "Making adversarial examples more transferable and indistinguishable," in *Proc. AAAI Conf. Artif. Intell.*, vol. 36, no. 3, 2022, pp. 3662–3670.

- [30] C. Xie, M. Tan, B. Gong, J. Wang, A. L. Yuille, and Q. V. Le, "Adversarial examples improve image recognition," in *Proc. IEEE/CVF Conf. Comput. Vis. Pattern Recog. (CVPR)*, 2020, pp. 819–828.
- [31] L. Rice, E. Wong, and Z. Kolter, "Overfitting in adversarially robust deep learning," in *Proc. Int. Conf. Mach. Learn. (ICML)*, 2020, pp. 8093–8104.
- [32] H. Zhang, Y. Yu, J. Jiao, E. Xing, L. El Ghaoui, and M. Jordan, "Theoretically principled trade-off between robustness and accuracy," in *Proc. Int. Conf. Mach. Learn. (ICML)*, 2019, pp. 7472–7482.
- [33] Y. Wang, D. Zou, J. Yi, J. Bailey, X. Ma, and Q. Gu, "Improving adversarial robustness requires revisiting misclassified examples," in *Proc. Int. Conf. Learn. Represent. (ICLR)*, 2020.
- [34] D. Wu, S.-T. Xia, and Y. Wang, "Adversarial weight perturbation helps robust generalization," in *Proc. Adv. Neural Inform. Process. Syst. (NeurIPS)*, vol. 33, 2020, pp. 2958–2969.
- [35] C. Luo, Q. Lin, W. Xie, B. Wu, J. Xie, and L. Shen, "Frequency-driven imperceptible adversarial attack on semantic similarity," in *Proc. IEEE/CVF Conf. Comput. Vis. Pattern Recog. (CVPR)*, 2022, pp. 15 315–15 324.
- [36] Y. Zhou, J. Huang, C. Wang, L. Song, and G. Yang, "Xnet: Wavelet-based low and high frequency fusion networks for fully-and semi-supervised semantic segmentation of biomedical images," in *Proc. IEEE/CVF Int. Conf. Comput. Vis. (ICCV)*, 2023, pp. 21 085–21 096.
- [37] Y. Luo, Y. Zhang, J. Yan, and W. Liu, "Generalizing face forgery detection with high-frequency features," in *Proc. IEEE/CVF Conf. Comput. Vis. Pattern Recog. (CVPR)*, 2021, pp. 16 317–16 326.
- [38] J. Fridrich and J. Kodovsky, "Rich models for steganalysis of digital images," *IEEE Trans. Inf. Forensics Security.*, vol. 7, no. 3, pp. 868–882, 2012.
- [39] S. A. Magid, Y. Zhang, D. Wei, W.-D. Jang, Z. Lin, Y. Fu, and H. Pfister, "Dynamic high-pass filtering and multi-spectral attention for image super-resolution," in *Proc. IEEE/CVF Int. Conf. Comput. Vis. (ICCV)*, 2021, pp. 4288–4297.
- [40] C. Xie, Y. Wu, L. v. d. Maaten, A. L. Yuille, and K. He, "Feature denoising for improving adversarial robustness," in *Proc. IEEE/CVF Conf. Comput. Vis. Pattern Recog. (CVPR)*, 2019, pp. 501–509.
- [41] E. Jang, S. Gu, and B. Poole, "Categorical reparameterization with gumbel-softmax," in *Proc. Int. Conf. Learn. Represent. (ICLR)*, 2016.
- [42] Z. Liu, Q. Liu, T. Liu, N. Xu, X. Lin, Y. Wang, and W. Wen, "Feature distillation: Dnn-oriented jpeg compression against adversarial examples," in *Proc. IEEE/CVF Int. Conf. Comput. Vis. (ICCV)*, 2019, pp. 860–868.
- [43] Y. Long, Q. Zhang, B. Zeng, L. Gao, X. Liu, J. Zhang, and J. Song, "Frequency domain model augmentation for adversarial attack," in *Proc. Eur. Conf. Comput. Vis. (ECCV)*, 2022, pp. 549–566.
- [44] L. Hu, L. Gao, Z. Liu, and W. Feng, "Temporal lift pooling for continuous sign language recognition," in *Proc. Eur. Conf. Comput. Vis. (ECCV)*, 2022, pp. 511–527.
- [45] J. Bai, L. Yuan, S.-T. Xia, S. Yan, Z. Li, and W. Liu, "Improving vision transformers by revisiting high-frequency components," in *Proc. Eur. Conf. Comput. Vis. (ECCV)*, 2022, pp. 1–18.
- [46] J. Zhang, X. Xu, B. Han, G. Niu, L. Cui, M. Sugiyama, and M. Kankanhalli, "Attacks which do not kill training make adversarial learning stronger," in *Proc. Int. Conf. Mach. Learn. (ICML)*, 2020, pp. 11 278–11 287.
- [47] A. Krizhevsky, G. Hinton *et al.*, "Learning multiple layers of features from tiny images," 2009.
- [48] J. Deng, W. Dong, R. Socher, L.-J. Li, K. Li, and L. Fei-Fei, "Imagenet: A large-scale hierarchical image database," in *Proc. IEEE/CVF Conf. Comput. Vis. Pattern Recog. (CVPR)*. IEEE, 2009, pp. 248–255.
- [49] S. Zagoruyko and N. Komodakis, "Wide residual networks," *arXiv preprint arXiv:1605.07146*, 2016.
- [50] K. He, X. Zhang, S. Ren, and J. Sun, "Deep residual learning for image recognition," in *Proc. IEEE/CVF Conf. Comput. Vis. Pattern Recog. (CVPR)*, 2016, pp. 770–778.
- [51] J. Cui, S. Liu, L. Wang, and J. Jia, "Learnable boundary guided adversarial training," in *Proc. IEEE/CVF Int. Conf. Comput. Vis. (ICCV)*, 2021, pp. 15 721–15 730.
- [52] W. J. Kim, Y. Cho, J. Jung, and S.-E. Yoon, "Feature separation and recalibration for adversarial robustness," in *Proc. IEEE/CVF Conf. Comput. Vis. Pattern Recog. (CVPR)*, 2023, pp. 8183–8192.
- [53] Z. Wei, Y. Wang, Y. Guo, and Y. Wang, "Cfa: Class-wise calibrated fair adversarial training," in *Proc. IEEE/CVF Conf. Comput. Vis. Pattern Recog. (CVPR)*, 2023, pp. 8193–8201.